Mechanism of GeO_2 resistive switching based on the multi-phonon assisted tunneling between traps

A. V. Shaposhnikov,[1] T. V. Perevalov,[1] V. A. Gritsenko,[1,a)] C. H. Cheng,[2] and A. Chin[2]
[1]*A.V. Rzhanov Institute of Semiconductor Physics, Siberian Branch of Russian Academy of Science, 13/Lavrentieva Ave., 630090 Novosibirsk, Russia*
[2]*Department of Electronics Engineering, National Chiao-Tung University, Hsinchu, Taiwan*

(Received 16 May 2012; accepted 31 May 2012; published online 14 June 2012)

Model of evenly distributed traps in bulk dielectric is proposed for the resistive memory switching mechanism. Switching from high resistance to the low resistance state is explained by several-fold increase in trap concentration after the application of switching voltage. Both high and low resistance conductivities are governed by multi-phonon ionization and tunneling between neighboring traps. Thermal trap energy for oxygen vacancy and electron effective mass for crystal α-GeO_2 were calculated using density functional theory and used for the fitting of our charge transport model of resistive memory. The model was verified on the TaN-GeO_2-Ni structure with good semi-quantitative agreement with experiment. © *2012 American Institute of Physics*. [http://dx.doi.org/10.1063/1.4729589]

Resistive random access memory (RRAM) has attracted considerable attention as the most promising candidate for the next generation of nonvolatile memory (NVM) due to superior characteristics, which include its simple metal–insulator–metal (MIM) structure, high density, fast write/erase switching times, low power consumption, and high endurance. Resistive memory is by six orders of magnitude faster than conventional flash memory with floating gate and has a switching time in the range of 1–10 ns, switching voltage in the range of 1–5 V, and the number of switching cycles 10^6–10^{12}. Switching from the high-resistance to the low-resistance states is obtained by applying of a short voltage pulse. Reverse transition occurs when an impulse of the longer duration is applied. Switching effect is observed in many dielectrics, such as SiO_2, GeO_2, HfO_2, TiO_2, Ta_2O_5, Nb_2O_5, organic films, and graphene oxide.

Considerable efforts were applied to the investigation of the switching mechanisms in RRAM, but its exact nature remains unclear.[1] In metal oxides, metallic filament conduction model is widely accepted.[2,3] According to this model, heating in high electric fields results in the fast diffusion of oxygen atoms, leading to the creation of conductive metallic filament. Creation of conductive filament results in the transition of the dielectric from high resistive state to the low resistive state. However, the high current passing through the metallic filament is opposite to the required low power in large memory arrays. Besides, the random formation of metallic filament is difficult to control with a wide range of resistance distribution, which is tough challenge to realize in high density memory arrays.

GeO_2 has attracted attention as a promising material for RRAM due to its high defect density[4] and small Ge-O bond formation energy.[5] Oxygen vacancies can be easily formed by interaction of GeO_2 with Ge at a very low temperature. The first non-metal-oxide Ni/GeO_x/TaN RRAM was reported at 2010.[6] In sharp contrast to conventional conductive filament RRAM, this device neither required a preforming process nor current compliance which simplifies the memory circuit design considerably. Besides, very low sub-μW power to high-resistance state (HRS) and even lower reset power of only sub-nW to low-resistance state (LRS) were achieved. Such GeO_x RRAM cannot be explained by metallic filament model because the GeO_x is a covalent-bond oxide rather than the metallic oxide. Moreover, the extremely low reset power cannot be explained by the model of disruption of conductive filament. The switching effect of this type of RRAM is thought to be related to the formation and annihilation of oxygen vacancies.

The purpose of this paper is to develop alternative non-filament physical model which will be able to adequately describe resistance switching effect in dielectrics. We propose a model for the resistive switching in RRAM based on the creation and annihilation of evenly distributed oxygen vacancies in the dielectric bulk.

For complementary metal-oxide-semiconductor transistor (CMOS) backend integration, a typical 0.5 μm isolation SiO_2 was deposited on 6-in. IC-standard Si substrate. Then TaN was deposited by physical vapor deposition (PVD) and patterned to form the bottom electrode. The GeO_x dielectric was deposited by PVD with a thickness of 12 nm. The top electrode was formed by nickel (Ni) deposition and patterning. The fabricated Ni/GeO_x/TaN devices were measured by DC current-voltage (I-V) set/reset, cycling, and retention at 85 °C under the similar charge-trapping flash memory tests.[7]

Fig. 1 shows the experimental hysteresis of current-voltage characteristics measured in HRS (curve 1) and LRS (curve 2). The current in the range 0–2.5 V of HRS curve 2 is related to the charge accumulation on traps in GeO_2. Current in the voltage range 2.5–4 V of LRS curve 1 exponentially increases with the voltage. At the high voltage of curve 1, GeO_2 sample is switched to the low-resistance state, with LgI-V characteristic described by curve 2 at the decreasing voltage. Very low self-compliance set current of -0.4 μA at -4 V (0.6 μW) to HRS, even lower reset current of only 16 pA at -1 V (16 pW) to LRS, and large HRS/LRS resistance window of 170 were achieved at 0.5 V read voltage. The HRS/LRS resistance window becomes larger and >500 at a read voltage of 1 V.

a)Author to whom correspondence should be addressed. Electronic mail: timson@isp.nsc.ru.

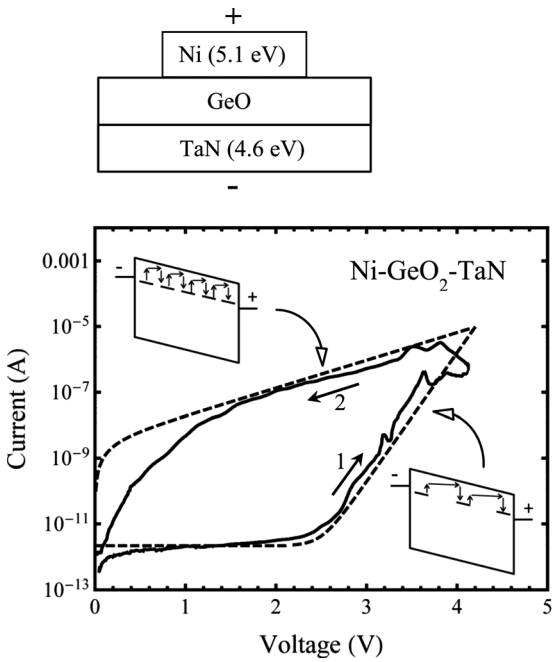

FIG. 1. Hysteresis of current-voltage characteristic in Ni-GeO_2-TaN structure (shown on the top) at room temperature. Curve 1 corresponds to HRS and measured at the rising ramp voltage. Curve 2 corresponds to LRS and measured at the decreasing ramp voltage. Solid lines represent experimental data, and dotted lines represent theoretically fitted curves. GeO_2 film thickness is 12 nm, Ni contact area is 1.13×10^{-4} cm^2. Insets in the lower and upper parts illustrate the picture of low and high trap concentration in high and low resistive states, respectively.

According to the proposed model, GeO_2 sample in the high resistance state has low concentration of traps (oxygen vacancies). In this state, charge transport is governed by the multi-phonon ionization and tunneling between traps (current in the voltage range 2.5–4 V on the curve 1).[8–11] This is illustrated by the inset in the lower part of Fig. 1.

Application of the high voltage results in many fold increase of traps concentration. Drastic increase in trap concentration results in exponential increase in tunneling probability of electrons between traps and therefore greatly increased current. This is illustrated by inset in the top of Fig. 1.

Quantitative theory of charge transport in dielectrics based on multi-phonon-assisted traps ionization and tunneling between traps was developed in Ref. 11. We have applied this model to describe charge transport both in high and low resistance states to explain resistive switching in GeO_2. In this model, phonon-assisted trap ionization and tunneling probability P is given by

$$P = \frac{\sqrt{\pi}\hbar W_t}{m^* N^{-\frac{2}{3}}\sqrt{2kT(W_{opt}-W_t)}} \exp\left(-\frac{W_{opt}-W_t}{2kT}\right) \times \exp\left(-\frac{2N^{-\frac{1}{3}}\sqrt{2m^*W_t}}{\hbar}\right) \sinh\left(\frac{eFN^{-\frac{1}{3}}}{2kT}\right). \quad (1)$$

Here, N is bulk trap concentration, W_t and W_{opt} are the thermal and optical energies of trap ionization, m* is the tunneling electron effective mass, $F = V/d$ is electric field, d is the thickness of dielectric, and T is the temperature. Compared to work in Ref. 11, we substituted hyper sinus with exponent in Eq. (1) to take into account probability for electron tunneling in the direction opposite to electric field.

In the first approximation, we neglect electric field non-uniformity in dielectric created by the space charge of carriers captured on traps. In the simplest one-dimensional model, the current density is given by the equation:

$$J = eN^{-\frac{2}{3}}P. \quad (2)$$

We used Eqs. (1) and (2) to fit experimental I-V curves, there high and low resistance states described by different trap concentration N_1 and N_2. According to formula (1), the slope of the LgI-V line allow us to determine the trap density in high resistive state ($N_1 = 6 \times 10^{18}\,cm^{-3}$) and low resistive state ($N_2 = 6 \times 10^{20}\,cm^{-3}$).

Fitting of experimental current-voltage characteristics requires us to know three more parameters: thermal W_t and optical W_{opt} trap energies and electron tunneling effective mass m^*. To further reduce the number of unknown free fitting parameters, we assumed relation $W_{opt} = 2W_t$. This relation was established for multi-phonon trap ionization model in the charge transport experiments for electrons and holes in Si_3N_4 (Refs. 12 and 13) and Al_2O_3.[14]

Unfortunately there is no available experimental data on the electron effective mass m^* and thermal ionization energy W_t. To obtain a good starting guess and verify that oxygen vacancy defect in GeO_2 indeed could be a trap for electrons, we conducted a first principle quantum-chemical simulation of a-quartz GeO_2.

Electronic structure of hexagonal GeO_2, with a structure similar to a-quartz, was investigated using plane-wave norm-conserving pseudopotential technique based on the first-principles density functional theory (DFT) in the quantum Espresso code.[15] Ground-state properties were obtained by minimizing the total energy. It is widely known that DFT approach, both in local density approximation (LDA) and gradient corrected approximation (GGA) consistently underestimate band gap of dialectics. Various techniques are used to address this shortcoming, including time-dependent DFT, many-particle GW approximation, and various hybrid DFT functionals, combining exact Hartry-Fock exchange with appropriate LDA/GGA formulation for electron correlation. The downside of all these methods is much higher demand on computational resources.

In this work, we used HSE hybrid functional to calculate electronic band structure of primitive GeO_2 cell with comparison of GGA PZ functional. Electronic structure of GeO_2 was calculated previously in the work.[16]

Band structure of GeO_2 was calculated for primitive trigonal cell, consisting of 3 Ge atoms and 6 O atoms, on the uniform Monkhorst-Pack grid of k-points with density of $10 \times 10 \times 10$. Fig. 2 presents the calculated band structure along high symmetry lines in the first Brilluene zone with HSE hybrid functional. While GGA potential expectedly underestimate band gap, HSE correctly predicts experimental value of 5.72 eV.[17] α-quartz GeO_2 is an indirect band gap dielectric with conduction band minimum in Gamma point and valence band maximum in M-point. Electron and hole effective masses were estimated from band structure calculations. Electron effective mass tensor is rather isotropic with

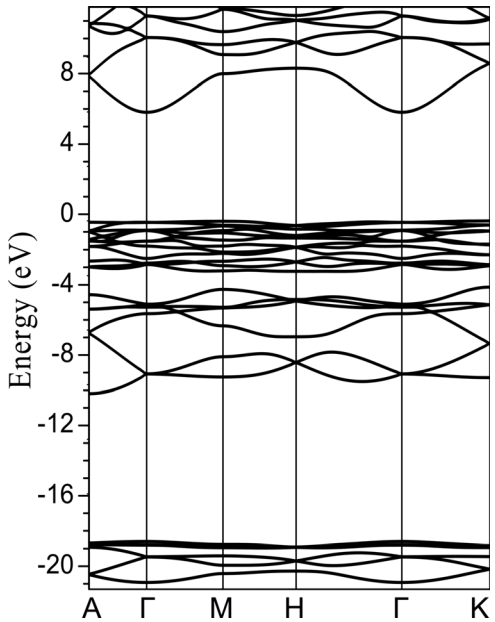

FIG. 2. Band structure of GeO_2 calculated with hybrid HSE potential along high symmetry lines in the first Brillouin zone of primitive 9-atom trigonal cell.

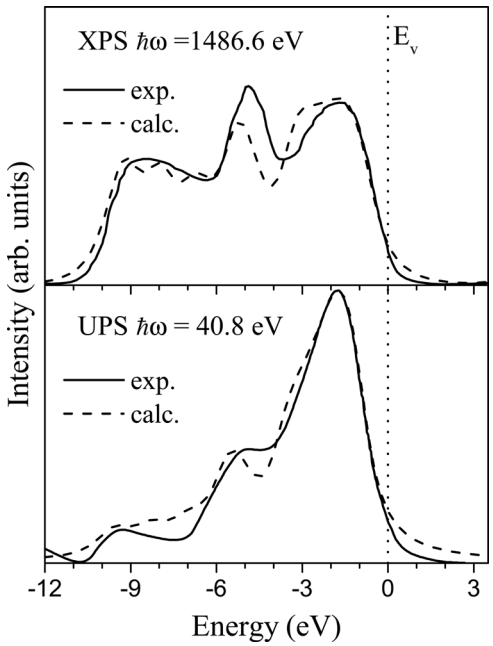

FIG. 3. Comparison of experimental UPS and XPS valence band spectra (solid line) of amorphous GeO_2 from Ref. 18 with calculated PDOS for α-GeO_2 (dotted line). Calculated PDOS for 4*s*, 4*p* valence states of Ge atom and 2*s*, 2*p* states for O atom weighed with experimental photoionization cross-section Ref. 19.

lowest mass $m^*_{\parallel} = 0.38\, m_e$ and highest $m^*_{\perp} = 0.48\, m_e$. Similar values were obtained for silicon nitride Si_3N_4.[12,13] Top of the valence band is rather flat (see Fig. 2) suggesting heavy holes with $m^*_h \sim 10\, m_e$.

Effective masses calculated within plain GGA DFT and with the use of more advanced hybrid functional do not differ much, to a degree of 10% which is beyond the precision attainable by our approach. This can be explained by the fact that energy correction due to inclusion of exact Hartry exchange for unoccupied levels is roughly the same for all k-vectors in the Brilluene zone. To obtain results suitable for direct comparison with experimental XPS and UPS spectra (Ref. 18), calculated partial density of states (PDOS) for 4*s*, 4*p* valence states of Ge atom and 2*s*, 2*p* states for O atom were weighed with experimental photoionization cross-section from Ref. 19 (Fig. 3). Again, PDOS calculated with HSE shows quite good agreement with experimental data.

For the calculation of electronic properties of oxygen vacancies, we constructed a 72 atom supercell, consisted of 8 primitive trigonal cells. Oxygen polyvacancies are created by removing one or more O atoms from within the same GeO_4 tetrahedron. To calculate the energy levels of vacancy defects, we calculated total energy of supercells with added or subtracted electron to the lowest unoccupied and highest occupied states, respectively. Long-range coulomb divergence is taken into account by the addition of compensating charge to obtain total cell charge neutrality.

Energy levels of defects in different charge states calculated using the following formula:

$$E_e = (E_d^{-1} - E_d^0) - (E_b^{-1} - E_b^0) \qquad (3)$$

There E_d represents the total energy of supercell with defect in various charged states, E_b is total energy of bulk supercell. Here, term $(E_d^{-1} - E_d^0)$ represent the energy difference between negatively charged and neutral defect supercell. This value is corrected with the electron affinity term $E_{aff} = (E_b^{-1} - E_b^0)$calculated for bulk supercell. Thus, all errors due to supercell approximation are effectively cancelled.

This technique allows us to estimate the energy level of electron traps in GeO_2, which corresponds to thermal trap energy W_t in multi-phonon trap ionization model described previously, $W_t = E_e$. Direct estimation of optical excitation energies requires us to calculate empty localized energy levels associated with the defect, taking into account electron subsystem relaxation due the electron excitation. This work is in progress. In this work, we estimated optical trap energy using experimental ratio $W_{opt}/W_t = 2$.[20,21]

Our results, obtained with GGA HSE functional for single oxygen vacancy, show the appearance of two localized electronic states in the band gap (Fig. 4). The low state has a bonding nature (σ), and the upper empty state is non-bonding (σ*). According to our model, electrons injected from contact (TaN) are captured by empty non-bonding localized states in the band gap of GeO_2. Subsequent

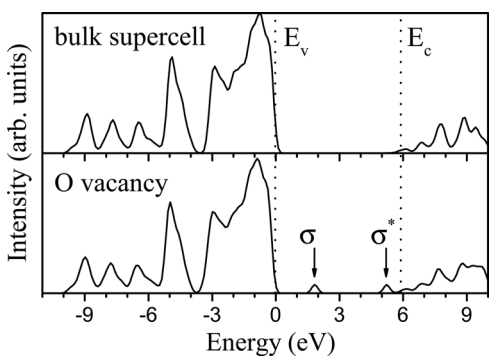

FIG. 4. Total density of states for bulk GeO_2 supercell and supercell with oxygen vacancy calculated with hybrid HSE potential.

electron multi-phonon assisted ionization and tunneling between neighboring traps provides low and high resistive conductivity of GeO_2.

Single oxygen vacancy in various dielectrics (SiO_2, Al_2O_3, ZrO_2, HfO_2, Ta_2O_3, TiO_2) is a widely acknowledged trap responsible for charge accumulation and excess leakage current. In this work, we assume single oxygen vacancy to be the primary defect responsible for RRAM switching mechanism. For the single oxygen vacancy, using hybrid HSE DFT potential, we calculated the value of trap thermal ionization energy W_t as 1.5 eV. Optical trap ionization energy can be estimated as $W_{opt} = 2W_t = 3.0$ eV.

Using the theoretically calculated values for $W_t = 1.5$ eV, $W_{opt} = 3$ eV, $m^* = 0.38\, m_e$ as the starting guess parameters, and values for concentration N in high ($N_1 = 6 \times 10^{18}\,\mathrm{cm}^{-3}$) and low resistive state ($N_2 = 6 \times 10^{20}\,\mathrm{cm}^{-3}$), using Eqs. (1) and (2), we obtained best fitting values for electron effective mass $m^* = 0.2\, m_e$ and trap thermal ionization energy $W_t = 1.42$ eV (Fig. 1).

The thermal energy $W_t = 1.42$ eV obtained from the fitting of experimental data to Eqs. (1) and (2) is in very good agreement with theoretically calculated energy for the oxygen vacancy defect $E_e = W_t = 1.5$ eV.

The obtained value for $m^* = 0.2\, m_e$ is close to the experimental values of tunnel effective masses in high-k dielectrics Al_2O_3 $0.28\, m_e$,[22] HfO_2 $0.1\, m_e$,[23] $0.17\, m_e$,[24] and Ta_2O_5 $0.3\, m_e$.[25] Theoretically calculated conduction band mass $m^* = 0.38\, m_e$ is twice as high as obtained fitting value. Experimental tunnel effective mass describe electron transport in the gap of dielectric, while theoretically calculated electron effective mass pertain to electron transport at the bottom of conduction band. This may explain the observed difference between tunnel and free electron effective mass in GeO_2. More detailed investigation is required.

Our theoretical model cannot adequately describe the experimental *LgI-V* low-resistance curve (2) in the low voltage range 0-1.5 V (see Fig. 1). This divergence can have two possible explanations. First, our simple model neglects the spatial charge distribution in dielectric created by carriers captured on traps. Second, we assume the existence of only one type of defect, namely single oxygen vacancy, described by single level in the gap. In real dielectrics, polyvacancies may play an important role. Polyvacancies can create multiple defect levels in the band gap, each characterized by its own value of energy level. Investigation of the possible role of polyvacancies in the dielectrics conduction mechanism is the topic for future work.

In conclusion, we proposed a simple model for describing resistive switching of RRAM dielectrics assuming the same multi-phonon assisted electron tunneling mechanism for both high resistance state and low resistance state. Switching from high resistive state to low resistive state is explained by the drastic increase in the concentration of traps and corresponding increase in electron tunneling probability between neighboring traps. We suggest that primarily trap in GeO_2 is an oxygen vacancy, which is the most widely acknowledged defect in dielectrics such as SiO_2, Al_2O_3, ZrO_2, HfO_2, Ta_2O_3, TiO_2. Using the proposed model, we obtained the value of trap thermal ionization energy $W_t = 1.42$ eV, which is in very good agreement with theoretically calculated energy level for oxygen vacancy 1.5 eV. Obtained value for electron tunnel effective mass $m^* = 0.2\, m_e$ is twice lower compared to theoretically calculated effective mass for the free conduction band electron but is close to experimentally determined tunnel effective masses for other high-k dielectrics.

This work was supported by the grant No. 24.18 of Russian Academy of Sciences, grant No. 5.12 of Siberian Branch of Russian Academy of Sciences and the National Science Council, Taiwan, under Grant No. NSC-100-2923-E-009-001-MY3. The computations were conducted at the Novosibirsk State University Supercomputer Center.

[1]G. I. Meijer, Science **319**, 1626 (2008).
[2]D.-H. Kwon, K. M. Kim, J. H. Jang, J. M. Jeon, M. H. Lee, G. H. Kim, X.-S. Li, G.-S. Park, B. Lee, S. Han, M. Kim, and C. Seong Hwang, Nat. Nanotechnol. **5**, 148 (2010).
[3]D. Ielimini, F. Nardi, and C. Cadli, Nanotechnology **22**, 254022 (2011).
[4]W. B. Chen and A. Chin, Appl. Phys. Lett. **95**, 212105 (2009).
[5]D. S. Yu, A. Chin, C. H. Wu, M.-F. Li, C. Zhu, S. J. Wang, W. J. Yoo, B. F. Hung, and S. P. McAlister, Tech. Dig. - Int. Electron Devices Meet. **2005**, 649.
[6]C. H. Cheng, A. Chin, and F. S. Yeh, Dig. Tech. Pap. - Symp. VLSI Technol. **2010**, 85.
[7]A. Chin, C. C. Laio, K. C. Chiang, D. S. Yu, W. J. Yoo, G. S. Samudra, S. P. McAlister, and C. C. Chi, Tech. Dig. – Int. Electron Devices Meet. **2005**, 165.
[8]S. D. Ganichev, E. Ziemann, W. Prettl, I. N. Yassievich, A. A. Istratov, and E. R. Weber, Phys. Rev. B **61**, 10361 (2000).
[9]E. Ziemann, S. D. Ganichev, W. Prettl, I. N. Yassievich, and V. I. Perel, J. Appl. Phys. **87**, 3843 (2000)
[10]S. D. Ganichev, I. N. Yassievich, and W. Prettl, J. Phys.: Condens. Matter **14**, R1263 (2002).
[11]K. A. Nasyrov and V. A. Gritsenko, J. Appl. Phys. **109**, 097705 (2011).
[12]S. Miyazaki, Y. Ihara, and M. Hirose, Phys. Rev. Lett. **59**, 125 (1987).
[13]V. A. Gritsenko, E. E. Meerson, and Yu. N. Morokov, Phys. Rev. B **57**, R2081 (1998).
[14]S. Meng, C. Basceri, B. W. Busch, G. Derderian, and G. Sandhu, Appl. Phys. Lett. **83**, 4429 (2003).
[15]P. Giannozzi, S. Baroni, N. Bonini, M. Calandra, R. Car, C. Cavazzoni, D. Ceresoli, G. L. Chiarotti, M. Cococcioni, I. Dabo, A. D. Corso, S. de Gironcoli, S. Fabris, G. Fratesi, R. Gebauer, U. Gerstmann, C. Gougoussis, A. Kokalj, M. Lazzeri, L. Martin-Samos, N. Marzari, F. Mauri, R. Mazzarello, S. Paolini, A. Pasquarello, L. Paulatto, C. Sbraccia, S. Scandolo, G. Sclauzero, A. P. Seitsonen, A. Smogunov, P. Umari, and R. M. Wentzcovitch, J. Phys.: Condens. Matter **21**, 395502 (2009).
[16]P. Broqvist, J. F. Binder, and A. Pasquarello, Appl. Phys. Lett. **94**, 141911 (2009).
[17]C. V. Ramanana, G. Carbajal-Franko, R. S. Vemuri, I. B. Troitskaia, S. A. Gromolov, and V. V. Atuchin, Mater. Sci. Eng., B **174**, 279 (2010).
[18]B. Fischer, R. A. Pollak, T. H. DiStefano, and W. D. Grobman, Phys. Rev. B **15**, 3193 (1977).
[19]J.-J. Yeh, *Atomic Calculation of Photoionization Cross-Sections and Asymmetry Parameters* (Gordon and Breach Science, Langhorne, 1993).
[20]K. A. Nasyrov, S. S. Shaimeev, V. A. Gritsenko, and J. H. Han, J. Appl. Phys. **105**, 123709 (2009).
[21]Yu. N. Novikov, V. A. Gritsenko, and K. A. Nasyrov, Appl. Phys. Lett. **94**, 222904 (2009).
[22]O. Blank, H. Reisinger, R. Stengl, M. Gutsche, F. Wiest, V. Capodieci, J. Schulze, and I. Eisele, J. Appl. Phys. **97**, 044107 (2005).
[23]W. J. Zhu, T.-P. Ma, J. Kim, and Y. Di, IEEE Electron Device Lett. **23**, 97 (2002).
[24]H. T. Takeuchi and T.-J. King, Appl. Phys. Lett. **83**, 788 (2003).
[25]M. Houssa, M. Tuominen, M. Naili, V. Afanas'ev, A. Stesmans, S. Haukka, and M. M. Heyns, J. Appl. Phys. **87**, 8615 (2000).